CFD and kinetic-based modeling to optimize the sparger design of a large-scale photobioreactor for scaling up of biofuel production

CFD and kinetic-based modelling to optimize the sparger design of a large-scale photobioreactor for scaling up of biofuel production

Haider Ali[1,2,3] and Cheol Woo Park[1†]

[1]*School of Mechanical Engineering, Kyungpook National University, 80 Daehakro, Bukgu, Daegu, 41566, Korea*

[21]*Department of Chemical Engineering, Imperial College London, South Kensington Campus, London SW7 2AZ, UK*

[3]*Department of Chemical Engineering, Norwegian University of Science and Technology (NTNU), Trondheim, NO-7491, Norway*

[†]*Corresponding author: Cheol Woo Park: Tel.:* +82 (53) 950 7569; *Fax:* +82 (53) 950 6550; *Email: chwoopark@knu.ac.kr*

Abstract

Microalgal biofuels have not yet achieved wide-spread commercialization, partially as a result of the complexities involved with designing and scaling up of their biosystems. The sparger design of a pilot-scale photobioreactor (120 L) was optimized to enable the scale-up of biofuel production. An integrated model coupling computational fluid dynamics and microalgal biofuel synthesis kinetics was used to simulate the biomass growth and novel biofuel production (i.e. bisabolene) in the photobioreactor. Bisabolene production from *Chlamydomonas reinhardtii* mutant was used as an example to test the proposed model. To select the optimal sparger configuration, a rigorous procedure was followed by examining the effects of sparger design parameters (number and diameter of sparger holes and gas flow rates) on spatially averaged bubble volume fraction, light intensity, friction velocity, power input, biomass concentration, and bisabolene production. The optimized sparger design increases the final biomass concentration by 18%, thereby facilitating the scaling up of biofuel production.

Keywords: biofuel, photobioreactor, scale-up, sparger design, CFD, kinetic modelling

1. Introduction

The global shift toward biomass-based renewable energy continues rapidly because of its sustainability and low environmental impact. Microalgae serve as the primary biomass source, with a production rate remarkably higher than those of other plant crops. Closed photobioreactors (PBRs) are one of the practical systems used for mass microalgal cultivation. PBRs prevent water evaporation and contamination with efficient temperature control and excellent light utilization (Chisti, 2007). Gas sparging is the most important factor to design and scale-up PBRs successfully because it directly affects mixing and light utilization (Gupta et al., 2015; Singh and Sharma, 2012). A sparger is used for bubbling gas from the bottom of the PBR to mix and degas the culture. The selection of the gas sparger is process specific, and to date, different types of spargers have been proposed, such as perforated plate, ring, and pipe. However, the type of sparger exhibits no significant difference in the hydrodynamic properties of the PBR (Luo et al., 2011). Gas sparging of the PBR remarkably depends on the inlet gas flow rates, frictional losses, algal biofouling, and the geometrical design parameters of the sparger (number, diameter, location, and orientation of holes). An increase in gas sparging rate enhances the mixing and degassing of culture in the PBR (Zhang et al., 2002). Nevertheless, increasing the gas sparging rates produces a large number of gas bubbles in the PBR, resulting in increased bubble scattering and reduced light utilization. Changing the number and diameter of sparger holes affects the liquid movement and mass transfer in the PBRs (Zhang et al., 2002; Zhang et al., 2015b). Gas bubbling in the PBR requires considerable power. The power input for gas bubbling depends on the inlet gas flow rates and pressure drop in the PBR. High sparging rates consume substantial power, making them infeasible for large-scale biomass production. Design parameters and biofouling of the sparger also

affect the power input because of their significant influence on the pressure drop (Béchet et al., 2013a; Chisti, 1998; Kulkarni et al., 2007).

Sparger-induced mixing ensures rapid transfer of CO_2 and nutrients, cell sedimentation prevention, uniform pH maintenance, and efficient gas exchange between microalgae culture and air (Carvalho et al., 2006; Luo and Al-Dahhan, 2004). Rapid mixing along the light penetration path enhances the photosynthetic efficiency of PBR by shifting algal cells between the light/dark cycles (Sforza et al., 2012). However, microalgal cells are sensitive to fluid dynamic stresses. Intensive mixing can cause shear-induced damage to these cells and consequently reduce their biomass productivity (Leupold et al., 2013; Michels et al., 2016; Thomas and Gibson, 1990). In addition to the bubble rising and bursting phenomena in the PBR, the bubble formation at the sparger could also damage algal cells (Barbosa et al., 2004). Shallow cultures utilize light more efficiently than dense cultures because of reduced light attenuation. Therefore, the scaling up of PBRs requires careful consideration of light attenuation, which is the decrease in local light intensity along the light penetration direction in the PBR. Light attenuation depends on the wavelength, PBR geometry, and light penetration distance. This result suggests that the local light intensity is significantly affected with microalgal cells concentration, gas bubble scattering, and light absorption by microalgal cells. Therefore, numerous PBR designs have been developed to increase light utilization by reducing the effects of gas bubble scattering and cell light absorption (Berberoglu et al., 2007; Fernandes et al., 2010; Molina Grima et al., 1994; Posten, 2009).

Advancements in the computational fluid dynamics (CFD) tools enable the modelling and improvement of biofuel production in industrial PBRs. A number of studies have been conducted to improve the PBR mixing by using baffles and specially designed mixers. Nonetheless, most of these studies focused only on the hydrodynamic or light regime characteristics of laboratory-scale

PBRs (less than 10 L), without including microalgal growth and biofuel production in their CFD models (Bergmann and Trösch, 2016; Chen et al., 2016; Huang et al., 2014; Huang et al., 2015; Su et al., 2010; Sun et al., 2016; Yang et al., 2016). Moreover, despite the importance of gas sparging in the design and scale-up of PBRs, only a few studies were conducted to investigate the influence of sparger design on mixing and light transmission in laboratory-scale PBRs (1 L) (Ranade and Tayalia, 2001; Zhang et al., 2015b). CFD modelling of hydrodynamics and growth kinetics (microalgae growth and biofuel production) in a large-scale PBR involves multiple scales, making it a highly complex and challenging task. Consequently, previous studies have been limited to investigating hydrodynamics and growth kinetics for large-scale cultures.

To fill this gap, the present study primarily aims to develop a hybrid model including CFD and microalgal growth kinetics to optimize the sparger design of a pilot-scale PBR (120 L) for scaling up of biofuel production. The biomass growth and biofuel (i.e. bisabolene in this study) production from *Chlamydomonas reinhardtii* were estimated with consideration of the influence of different sparger design parameters. A genetically modified *C. reinhardtii* strain was used to produce excreted biofuel (*i.e.* bisabolene in this study (del Rio-Chanona et al., 2019; Wichmann et al., 2018)). Results of the CFD model were validated using experimental results of biomass concentration and bisabolene production. Sparger design was optimized by analyzing and determining the effects of sparger design parameters (number and diameter of sparger holes and gas flow rates) on spatially averaged bubble volume fraction, light intensity, friction velocity, power input, biomass concentration, and bisabolene production. The loss in PBR productivity related to shear-induced cell damage (dead zones) was also taken into account. An empirical correlation was specifically developed to estimate the bubble volume fraction using the sparger

93 design parameters in large-scale PBRs, with consideration of effects of bubble scattering on the
94 local light intensity.

95 **2. Mathematical modelling**

96 The CFD model of the 120 L pilot-scale flat-plate PBR (Department of Chemical Engineering of
97 Imperial College London, UK) was constructed and is shown in Figure 1. The liquid
98 compartment contains the microalgal culture; its dimension shows a width (*W*) of 1700 mm,
99 height (*H*) of 900 mm, and depth (*D*) of 67 mm. A sparger (diameter = 20 mm and width = 1600
100 mm) is used to inject recycling gas into the liquid compartment from the bottom of the PBR to
101 mix the culture and supply CO_2. A full factorial design (2^3) was implemented to generate eight
102 possible design configurations of the sparger based on the number and diameter of sparger holes
103 and recycling gas flow rates (Table 1). It is noticeable that once the number of holes was
104 determined, the hole pitch was also fixed automatically in this study, given the assumption that
105 holes are evenly distributed on the sparger surface. The present study assumed that the microalgal
106 cell movement is approximately same as the bulk movement of liquid because of the negligible
107 difference between liquid and biomass densities (Zhang et al., 2015b). Therefore, the gas bubbles
108 rising from the PBR bottom induce a circulatory motion in the liquid culture because of the
109 buoyancy effect; this phenomenon represents a two-phase gas–liquid flow mixing problem (Becker
110 et al., 1994).

111 **2.1. Hydrodynamic modelling**

112 The Euler–Euler method solves the average phase concentrations; thus, it was used to model the
113 gas–liquid flow in the PBR (Becker et al., 1994; Lestinsky et al., 2012). The continuity equations
114 for liquid and gas phases are expressed as follows:

$$\frac{\partial}{\partial t}\varphi_l\rho_l + \nabla(\varphi_l\rho_l U_l) = 0 \quad (1)$$

$$\frac{\partial}{\partial t}\varphi_g U_g + \nabla\left(\rho_g\varphi_g U_g\right) = \mathrm{m_{gl}} \quad (2)$$

where φ_l is the liquid volume fraction (1), ρ_l is the liquid density (kg/m^3), U_l is the liquid velocity (m/s), φ_g is the gas bubble volume fraction (1), U_g is the gas velocity (m/s), ρ_g is the gas density (kg/m^3), ∇ is the gradient operator ($\frac{\partial}{\partial \mathrm{x}}, \frac{\partial}{\partial \mathrm{y}}, \frac{\partial}{\partial \mathrm{z}}$), and $\mathrm{m_{gl}}$ is the interfacial mass transfer rate (kg/m^3·s). The gas bubble volume fraction or holdup is the total volume of gas retained in the PBR at a given time. The governing equations of the momentum for liquid and gas phases are as follows:

$$\frac{\partial}{\partial t}(\varphi_l\rho_l U_l) + \nabla(\varphi_l\rho_l U_l U_l) = -\varphi_l\nabla p + \nabla\cdot\varphi_l[\mu_l(\nabla U_l + (\nabla U_l)^T)] + \varphi_l\rho_l \mathrm{g} \quad (3)$$

$$\frac{\partial}{\partial t}\left(\varphi_g\rho_g U_g\right) + \nabla\left(\varphi_g\rho_g U_g U_g\right) = -\varphi_g\nabla p + \nabla\cdot\varphi_g\left[\mu_g\left(\nabla U_g + \left(\nabla U_g\right)^T\right)\right] + \varphi_g\rho_g \mathrm{g} \quad (4)$$

where p is the pressure (Pa), μ_l is the liquid dynamic viscosity (Pa·s), g is the gravity vector (9.81 m/s^2), and μ_g is the gas dynamic viscosity (Pa·s). Liquid volume fraction (φ_l) and gas velocity (U_g) are defined as follows (Sokolichin et al., 2004):

$$\varphi_l = 1 - \varphi_g \quad (5)$$

$$U_g = U_l + U_{slip} \quad (6)$$

where U_{slip} represents the slip velocity (m/s). The Euler–Euler model uses the following equations to calculate slip velocity (U_{slip}) (Sokolichin et al., 2004):

$$\frac{3}{4}\frac{C_{\mathrm{d}}}{d_{\mathrm{b}}}\left|U_{slip}\right|U_{slip} = -\nabla p \tag{7}$$

$$C_{\mathrm{d}} = \frac{0.622}{\frac{1}{\mathrm{E\ddot{o}}} + 0.235} \tag{8}$$

$$\mathrm{E\ddot{o}} = \frac{\mathrm{g}\rho_l {d_{\mathrm{b}}}^2}{\sigma} \tag{9}$$

where C_{d} denotes the drag coefficient (1), d_{b} represents the gas bubble diameter (0.008 m in this study measured through experiments), and σ refers to the surface tension coefficient (0.07 N/m, commonly used in the water–air system (Pallas and Harrison, 1990)).

The *k*–*ε* turbulence model was used to model the turbulence generated in the PBR. The turbulent kinetic energy (k_t) and the dissipation rate (ε) equations are as follows:

$$\frac{\partial}{\partial t}(\rho_l k_t) + \rho_l U_l \cdot \nabla k_t = \nabla \cdot \left[\left(\mu_l + \frac{\mu_T}{\sigma_k}\right)\nabla k_t\right] + \frac{1}{2}\mu_T(\nabla U_l + (\nabla U_l)^T)^2 - \rho_l \varepsilon - C_k \varphi_g \nabla p \cdot U_{slip} \tag{10}$$

$$\frac{\partial}{\partial t}(\rho_l \varepsilon) + \rho_l U_l \cdot \nabla \varepsilon = \nabla \cdot \left[\left(\mu_l + \frac{\mu_T}{\sigma_\varepsilon}\right)\nabla \varepsilon\right] + \frac{1}{2}C_{\varepsilon 1}\frac{\varepsilon}{k}\mu_T(\nabla U_l + (\nabla U_l)^T)^2 - \rho_l C_{\varepsilon 2}\frac{\varepsilon^2}{k} - \frac{\varepsilon}{k}C_\varepsilon C_k \varphi_g \nabla p \cdot U_{slip} \tag{11}$$

$$\mu_T = \frac{\rho_l C_\mu {k_t}^2}{\varepsilon} \tag{12}$$

where μ_T represents the dynamic viscosity (Pa·s), C_k (0.505) refers to the bubble-induced turbulence parameter, σ_k (1) and σ_ε (1.3) represent the turbulent Prandtl numbers, and $C_{\varepsilon 1}$ (1.44)

148 and $C_{\varepsilon 2}$ (1.92) denote the first and second experimental model constants, respectively. The k–ε
149 turbulence model uses the experimentally derived values of these model constants (Wilcox,
150 2006).
151 Friction velocity is a classical form to represent shear stress in units of velocity, and it helps to
152 estimate the shear rate in a flow. Therefore, friction velocity was used to evaluate the shear
153 stresses imposed on the microalgae in the PBR. The friction velocity can be expressed as follows
154 (Leupold et al., 2013; Michels et al., 2016):

155 $$U_f = \left(\frac{\tau_s}{\rho_l}\right)^{1/2} \quad (13)$$

156 where U_f is the friction velocity (cm/s), and τ_s is the shear stress (Pa). A friction velocity higher
157 than 1 cm/s damages *C. reinhardtii* cells and decreases their photosynthetic efficiencies (Leupold
158 et al., 2013; Michels et al., 2016). The decrease in the photosynthetic efficiency caused by high
159 friction velocity (> 1 cm/s) reduces the PBR productivity. The loss in PBR productivity was
160 estimated by calculating the productive and unproductive volumes of the reactor. The productive
161 volume is the PBR region that produces biofuel and exhibits a local friction velocity of less than
162 1 cm/s. The unproductive or dead zone volume can be defined as the region with no biofuel
163 production but with local friction velocity higher than 1 cm/s. Apart from that dead zone can also
164 mean the region where culture mixing is too slow to maintain an effective biomass movement.
165 Thus, cells are stagnant and not able to receive nutrients promptly. However, it was confirmed by
166 previously published experimental results that culture mixing is maintaining an effective biomass
167 movement in the photobioreactor (Harun et al., 2018; del Rio-Chanona et al., 2019; Zhang et al.,
168 2015a; Zhang et al., 2015c; Zhang et al., 2015b). These results imply that dead zones due to low
169 culture mixing were not observed in the experiments. Thus, all the parameters used in the present

study were derived from previous experimental data to ensure effective biomass movement. For this reason, it was assumed that the dead zones due to low culture mixing are negligible and thus were not discussed in the present study. The loss in PBR productivity was calculated using the following equation:

$$Productivity\ loss\ (\%) = \frac{\text{Unproductive or dead zone volume (L)}}{PBR\ total\ volume\ (L)} \times 100 \quad (14)$$

2.2. Microalgal growth and bisabolene production modelling

In our recent study, a kinetic model was proposed to simulate microalgae biomass growth and bisabolene production from a genetically modified *C. reinhardtii* strain (Harun et al., 2018; del Rio-Chanona et al., 2019). The study used the logistic model (Dechatiwongse et al., 2014; del Rio-Chanona et al., 2017; del Rio-Chanona et al., 2019) to simulate the biomass growth rate in the PBR with the assumption that nutrients are supplied in excess. The logistic model defines the biomass growth rate as follows:

$$\frac{dX}{dt} = \mu \cdot X - \mu_d \cdot X^2 + \nabla \cdot (U_l \cdot X) \quad (15)$$

where X is the biomass concentration (g/L), μ is the biomass specific growth rate (1/h), and μ_d is the biomass specific decay rate (L/g/h). The biomass specific growth rate (μ) depends on the light intensity and culture temperature. The Aiba and Arrhenius models (Zhang et al., 2015a) were used to simulate the influences of light intensity and temperature on biomass growth, respectively. The governing equations of biomass specific growth rate (μ), light intensity (I), and culture temperature (T) can be written as follows:

$$\mu = \mu_m \cdot k(I) \cdot k(T) \quad (16)$$

$$k(I) = \frac{I(t,z)}{I(t,z) + k_s + \frac{I^2(t,z)}{k_i}} \quad (17)$$

$$k(T) = \exp\left[-\left(\frac{E_a}{RT} - \frac{E_a}{RT_a}\right)\right] - \exp\left[-\left(\frac{E_b}{RT} - \frac{E_b}{RT_b}\right)\right] \quad (18)$$

where μ_m represents the maximum biomass specific growth rate (0.304 1/h), $I(z)$ refers to the local light intensity (μE/m^2/s), k_s denotes the photosaturation term (34.92 μE/m^2/s), k_i represents the photoinhibition term (441.2 μE/m^2/s), E_a refers to the algal activation energy (144 kJ/mol), E_b denotes the algal deactivation energy (343.9 kJ/mol), and T_a (306.7 K) and T_b (307.1 K) refer to the reference temperatures. All the parameter values were obtained from the recent study (Harun et al., 2018; del Rio-Chanona et al., 2019).

Light distribution within photobioreactor can be influenced by scattering, reflection, and refraction of light caused by the algae cells, liquid medium, gas bubbles, and reactor geometry. Nevertheless, it is not possible to include the effects of these parameters into a single model. Lambert-Beer law is one of the existing models that comprehensively consists of the light scattering and absorption effects by gas bubbles and algae cells. Light attenuation remains dependent on light penetration distance, which suggests that the local light intensity ($I(t,z)$) is affected by cell absorption and bubble scattering (Zhang et al., 2015b). Therefore, the local light intensity experienced by microalgal cells in the culture is much lower than the incident light intensity. The modified Lambert–Beer's law was used to model the local light intensity by taking into account the microalgal cell absorption and bubble scattering (Béchet et al., 2013b; Zhang et al., 2015b). The governing equation of the local light intensity ($I(t,z)$) includes both spatial (light transmission direction) and time dimensions and is given as follows:

$$I(t,z) = I_0(t,z) \cdot \exp[-(\tau \cdot X(t,z) + K_a) \cdot z] \quad (19)$$

where I_0 is the incident light intensity (60 μE/m^2/s), τ is the algal cell absorption coefficient (33.9 m^2/g), K_a is the bubble scattering coefficient (1/m), and z is the distance from the light source (m). K_a is defined using the following equation (Zhang et al., 2015b):

$$K_a = \frac{3\varphi_g}{d_\mathrm{b}} \tag{20}$$

The bubble volume fraction was calculated using the CFD model and then imported to the kinetic model for evaluating light intensity. Bisabolene production in the PBR was simulated using the modified Luedeking–Piret model (Mu et al., 2015). The governing equation of the bisabolene production is shown as follows:

$$\frac{dP}{dt} = \left(Y_1 \cdot \frac{dX}{dt} + Y_2 \cdot X\right) \cdot \left(\alpha - k(T)\right) \tag{21}$$

where P is the bisabolene production (μg/L), Y_1 is the biomass growth-associated bisabolene yield coefficient (326.7 μg/g), Y_2 is the biomass growth-independent bisabolene yield coefficient (1.758 μg/g/h), and α is the temperature-dependent bisabolene synthesis rate (0.474). The values of the parameters used in mathematical modelling were derived from previous experimental data (Harun et al., 2018). A detailed introduction of the kinetic model can be found in our previous work (del Rio-Chanona et al., 2019).

COMSOL Multiphysics (5.3a, COMSOL Inc., Burlington, MA, USA) was used to estimate the gas–liquid flow mixing, microalgal growth, and bisabolene production in the pilot-scale PBR. The computational fluid dynamics (CFD model) was simulated using the turbulent bubbly flow interface of COMSOL Multiphysics. Then, the liquid velocity from the CFD model is imported to the biochemical reaction kinetics (kinetic model), and these are simulated using the partial differential equation (PDE) interfaces of COMSOL Multiphysics. A transient solver was used to solve the turbulent bubbly flow and the PDE interfaces of COMSOL Multiphysics for 40 h. The

time-dependent approach helps the hybrid model to compute and compare biomass growth and bisabolene production with previous experimental data (Harun et al., 2018) at different time intervals. This approach makes it more realistic than the steady-state simulation. Moreover, the computational time in this particular study largely depends on grid size and less on simulation type (transient or steady-state), keeping in view the large volume of the photobioreactor (120 L). The results of grid independency test, light intensity, and power input are presented in Appendix-A. For complex systems such as photobioreactors, averaging the spatial distribution of the parameters (bubble volume fraction, light intensity, friction velocity, power input, biomass concentration, and bisabolene production) is a reasonable approach to effectively present the results for better understanding (Fernández et al., 2014; de Mooij et al., 2016).

3. Experimental validation

The proposed CFD and kinetic-based model was initially compared and validated using previously published experimental data obtained from a 1 L lab-scale PBR (Harun et al., 2018; del Rio-Chanona et al., 2019; Zhang et al., 2015b; Zhang et al., 2015a). The biomass concentration and bisabolene production were simulated in a 1 L PBR with a W of 200 mm, H of 140 mm, and D of 25 mm. The sparger (diameter = 5 mm and W = 200 mm) with 20 holes (diameter of holes = 1 mm) was used to provide recycling gas at a velocity of 0.47 m/s from the bottom of the PBR. The lab-scale PBR was discretized with; a tetrahedral grid type and grid size of 94,850 domains, 8,266 boundaries, and 380 edge elements. The proposed CFD and kinetic-based model in this study (described in section 2) was used to estimate gas–liquid flow mixing, microalgal growth, and bisabolene production in the lab-scale PBR. The values of all parameters used in the simulations were obtained from the experimental results (Harun et al., 2018; Zhang et al., 2015a). The average bubble volume fraction of the present study was 0.00614, which is close

to that of the experimentally calculated bubble volume fraction (0.0067) (Zhang et al., 2015a). The maximum difference between the modelling (present study) and experimental (Harun et al., 2018; Zhang et al., 2015b) results of biomass concentration was 3.94% at the 65th h, and that of the bisabolene production is 10.99% at the 73rd h (Figures 2(a) and 2(b)). The present results are in reasonable agreement with the experimental results, thereby verifying the accuracy of the developed CFD and kinetic-based model.

4. Results and discussion

4.1. Bubble volume fraction

Local light intensity depends on gas bubble scattering, and its uniform distribution in the PBR is essential for microalgal growth. However, a significant difference in bubble volume fraction changes the uniformity of local light intensity (Zhang et al., 2015b). Varying the number and diameter of sparger holes remarkably affects the bubble volume fraction (Figure 3(a)). An increase in the number of sparger holes decreases the bubble volume fraction in the PBR. Increasing the diameter of holes results in a manner similar to that when increasing the number of holes. Increasing the recycling gas flow rate also increases the bubble volume fraction, which consequently enhances the culture mixing in the PBR. This increased mixing rate helps in the transfer of nutrients to microalgal cells. Nevertheless, a substantial increase in the bubble volume fraction can reduce the distribution of local light intensity in the PBR. Therefore, a balance must be maintained in the selection of the number and diameter of sparger holes to ensure that bubble volume fraction may not significantly affect the local light intensity. Therefore, the number and diameter of holes and gas flow rate in the range of 92–104, 1.0–2.5 mm, and 14.5–17.5 L/min, respectively, are suitable in generating bubble volume fraction of 0.0055 in the current pilot-scale PBR.

4.2. Empirical correlation for bubble volume fraction

Developing an empirical correlation can be helpful in selecting the optimal bubble volume fraction to reduce the effects of bubble scattering on the local light intensity and generate effective mixing in the PBR. Integrating the empirical correlation for bubble volume fraction with Lambert–Beer's law (Equation 19 and Equation 20) enables the modelling of the light transmission in the PBR. The number of parameters on which the bubble volume fraction in the 120 L PBR may depend on was determined via dimensional analysis. The bubble volume fraction depends on the number of sparger holes (N_H), sparger hole diameter (D_H), sparger hole pitch (P_H), sparger diameter (D_s), bubble diameter (d_b), and Reynolds number (Re). The empirical correlation for the bubble volume fraction (φ_g) in pilot-scale PBR was obtained using Buckingham's π theorem, and it can be written as follows based on the present simulation data (shown in Figure 4):

$$\varphi_g = C_o \left(\frac{1}{N_H}\right)^a \left(\frac{d_\mathrm{b}}{D_H}\right)^b \left(\frac{P_H}{D_s}\right)^c (\mathrm{Re})^d \tag{22}$$

$$Re = \frac{U_g D_\mathrm{h}}{\upsilon} \tag{23}$$

$$D_\mathrm{h} = \frac{4WD}{2(W+D)} \tag{24}$$

where υ is the kinematic viscosity of liquid, U_g is the gas velocity, and D_h is the hydraulic diameter of the PBR (m) (Ratchford and Fallowfield, 1992). Additionally, C_o is the constant, and a, b, and c are the exponents to be calculated using nonlinear regression analysis. The empirical correlation for the bubble volume fraction can be written in the following form after calculation of the pending coefficients:

$$\varphi_g = 0.0018 \left(\frac{1}{N_H}\right)^{-0.0164} \left(\frac{d_\mathrm{b}}{D_H}\right)^{0.0326} \left(\frac{P_H}{D_s}\right)^{0.2587} (Re)^{0.0065}, \quad R^2 = 0.99 \tag{25}$$

The empirical correlation (Equation 25) used to calculate the bubble volume fraction was valid for $62 \leq N_H \leq 122$, $1 \leq D_H \leq 5$ mm, $13 \leq P_H \leq 26$ mm, and $3.5\times10^4 \leq Re \leq 1.4\times10^5$. Results were plotted with the CFD data (Figure 4). A close agreement is observed between the results of the bubble volume fraction calculated using the empirical correlation and the CFD data. The standard error is approximately 0.77%. These results confirmed that the proposed empirical correlation (Equation 25) can be used to compute the bubble volume fraction in large-scale PBR effectively and consequently determine the local light intensity.

4.3. Friction velocity

A detailed investigation on the effects of friction velocity (shear stress) on algal cells is necessary for the design and scale-up of PBRs. PBR sparger exerts a major influence on the friction velocity because of its direct relationship with mixing (Figure 5). Increasing the number and diameter of sparger holes reduces the effects of friction velocity on algae cells. By contrast, the friction velocity increases when the sparger operates at high gas flow rates. High gas sparging rates produce a large number of bubbles that improve culture mixing by prompting the liquid circulation in the PBR. Bursting of these large number of bubbles increases the friction velocity and consequently reduces the photosynthetic efficiency of algae cells. However, the friction velocities presented in the Figure 5 are their average values. These results imply that despite the value of average friction velocity less than 1 cm/s (Figure 5), there could be regions in the PBR with the local friction velocity higher than 1 cm/s. Thus, it is essential to quantify the local friction velocity and productive volume of the PBR. The productive and unproductive or dead zone volumes resulting from the different sparger designs were also estimated (Table 2). The productive volume of the PBR is at maximum (productivity loss of only 1.66%) when the recycling gas is provided using sparger design 3 (number of holes = 122, hole diameter = 1 mm,

and recycling gas flow rate = 5 L/min). The sparger design 3 results in better productive volume than the other sparger designs because of the minimum dead zones produced by a large number of holes and low gas flow rate. The maximum productivity loss is observed at sparger designs 2 (number of holes = 62, hole diameter = 1 mm, and recycling gas flow rate = 20 L/min) and 6 (number of holes = 62, hole diameter = 5 mm, and recycling gas flow rate = 20 L/min), thereby indicating their unsuitability in biofuel production. This study effectively assumed and estimated the unproductive regions in the PBR. However, in actual conditions, the mixing forces the algal cells to move through the entire reactor. Thus, the damaged cells from the unproductive regions would still be unproductive in the rest of the system that eventually causes the death of the whole culture, unless growth exceeds this. These results suggested that the number and diameter of holes and gas flow rate in the range of 115–122, 4.5–5.0 mm, and 5.0–7.5 L/min, respectively, are potentially suitable with optimized friction velocity (0.66 m/s).

4.4. Biomass concentration and bisabolene production

Finally, the effects of the sparger design parameters (number and diameter of sparger holes and gas flow rate) on average biomass concentration and bisabolene production were estimated and analyzed. The biomass concentration decreases with an increase in the number and diameter of sparger holes (Figure 6). This decrease in biomass concentration indicates the low liquid circulation in the PBR due to the use of a large number and diameter of sparger holes. Increasing the gas flow rates improves the liquid circulation in the PBR, which consequently increases the biomass concentration. Increasing the number and diameter of sparger holes and gas flow rates affects the bisabolene production in manner similar to that on the biomass concentration. Although, using the minimum hole number and diameter and maximum gas flow rate significantly improves the mixing which in turn increases the biomass concentration and bisabolene

346 production. The local friction velocity is higher than 1 cm/s for these sparger design parameters. In
347 actual conditions, the biomass concentration and bisabolene production must decrease using the
348 minimum hole number and diameter and maximum gas flow rate because the friction velocity
349 exceeds 1 cm/s. However, the proposed model has a limitation that it cannot automatically reduce
350 the biomass concentration and bisabolene production when the frictional velocity reaches beyond
351 the critical value (1 cm/s). Thus, to optimize the biomass concentration (0.6 g/L) and bisabolene
352 production (25.05 µg/L) in the current pilot-scale PBR and meanwhile to consider the impact of
353 hydrodynamics on cell damage, the number and diameter of holes and gas flow rates should be
354 fixed in the range of 115–122, 4.5–5.0 mm, and 5.0–7.5 L/min (Figure 6), respectively.

355 **5. Conclusion**

356 This study implemented a CFD and algal growth kinetic-based model to optimize the sparger
357 design for a 120 L pilot-scale PBR. The effects of different sparger designs on biomass growth
358 and biofuel production were examined. The optimized sparger design parameters (number and
359 diameter of holes and gas flow rate) were selected based on their effects on bubble volume
360 fraction, average light intensity, friction velocity, power input, biomass concentration, and
361 bisabolene production. The PBR productivity loss due to cell damage (dead zones) was
362 calculated. A new empirical correlation was proposed to estimate the bubble volume fraction in
363 large-scale PBRs.

364 The present study found that the sparger design significantly affected biofuel production in the
365 pilot-scale PBR. The number and diameter of sparger holes were inversely related to the bubble
366 volume fraction, friction velocity, biomass concentration, and bisabolene production, but gas
367 flow rate was directly related to them. Providing recycling gas to the PBR under high flow rates
368 improved culture mixing, however, it also required substantial power. The increase in bubble

volume fraction significantly increased the culture mixing, but it also disturbed local light intensity and induced shear stresses on algal cells. The proposed empirical correlation effectively estimated the bubble volume fraction, and it can be helpful in determining the local light intensity in the PBR by integrating the light transmission equations (Equation 19 and Equation 20). The increased liquid circulation due to high gas flow rate also increased the shear-induced cell damage (dead zones), as shown by the substantial productivity losses of the PBR. To scale up the biofuel production process, this study recommends the optimized number and diameter of sparger holes and gas flow rate to be in the range of 115–122, 4.5–5.0 mm, and 5.0–7.5 L/min, respectively. It may be possible in future, that a shear stress-related condition could be included in the proposed hybrid model that permits it to automatically decrease the biofuel production when the friction velocity exceeds 1 cm/s. Furthermore, keeping in view the scaling-up of PBRs, it is encouraged to develop an empirical model for biofuel production correlating different parameters (bubble scattering, reactor geometry, light intensity, temperature, growth rates, etc.).

Acknowledgements

This study was supported by a National Research Foundation of Korea (NRF) grant funded by the Korea government (MSIP) (No. 2017R1A2B2005515), and a grant from the Priority Research Centers Program through the NRF, as funded by the MEST (No. 2010-0020089).

Declaration of interest: none

References

Barbosa MJ, Hadiyanto, Wijffels RH. 2004. Overcoming Shear Stress of Microalgae Cultures in Sparged Photobioreactors. *Biotechnol. Bioeng.* **85**:78–85.

Béchet Q, Muñoz R, Shilton A, Guieysse B. 2013a. Outdoor cultivation of temperature-tolerant

Chlorella sorokiniana in a column photobioreactor under low power-input. *Biotechnol. Bioeng.* **110**:118–126.

Béchet Q, Shilton A, Guieysse B. 2013b. Modeling the effects of light and temperature on algae growth: State of the art and critical assessment for productivity prediction during outdoor cultivation. *Biotechnol. Adv.* **31**:1648–1663.

Becker S, Sokolichin a., Eigenberger G. 1994. Gas—liquid flow in bubble columns and loop reactors: Part II. Comparison of detailed experiments and flow simulations. *Chem. Eng. Sci.* **49**:5747–5762.

Berberoglu H, Yin J, Pilon L. 2007. Light transfer in bubble sparged photobioreactors for H2production and CO2mitigation. *Int. J. Hydrogen Energy* **32**:2273–2285.

Bergmann P, Trösch W. 2016. Repeated fed-batch cultivation of Thermosynechococcus elongatus BP-1 in flat-panel airlift photobioreactors with static mixers for improved light utilization: Influence of nitrate, carbon supply and photobioreactor design. *Algal Res.* **17**:79–86.

Carvalho AP, Meireles LA, Malcata FX. 2006. Microalgal Reactors: A Review of Enclosed System Designs and Performances. *Biotechnol. Prog.* **22**:1490–1506.

Chen Z, Jiang Z, Zhang X, Zhang J. 2016. Numerical and experimental study on the CO2 gas–liquid mass transfer in flat-plate airlift photobioreactor with different baffles. *Biochem. Eng. J.* **106**:129–138.

Chisti Y. 1998. Pneumatically Agitated Bioreactors in Industrial and Environmental Bioprocessing: Hydrodynamics, Hydraulics, and Transport Phenomena. *Appl. Mech. Rev.* **51**:33.

Chisti Y. 2007. Biodiesel from microalgae. *Biotechnol. Adv.* **25**:294–306.

Dechatiwongse P, Srisamai S, Maitland G, Hellgardt K. 2014. Effects of light and temperature on the photoautotrophic growth and photoinhibition of nitrogen-fixing cyanobacterium Cyanothece sp. ATCC 51142. *Algal Res.* **5**:103–111.

Fernandes BD, Dragone GM, Teixeira JA, Vicente AA. 2010. Light regime characterization in an airlift photobioreactor for production of microalgae with high starch content. *Appl.*

419 *Biochem. Biotechnol.* **161**:218–226.

420 Fernández I, Acién FG, Berenguel M, Guzmán JL. 2014. First Principles Model of a Tubular
421 Photobioreactor for Microalgal Production. *Ind. Eng. Chem. Res.* **53**:11121–11136.

422 Gupta PL, Lee S-M, Choi H-J. 2015. A mini review: photobioreactors for large scale algal
423 cultivation. *World J. Microbiol. Biotechnol.* **31**:1409–1417.

424 Harun I, Del Rio-Chanona EA, Wagner JL, Lauersen KJ, Zhang D, Hellgardt K. 2018.
425 Photocatalytic Production of Bisabolene from Green Microalgae Mutant: Process Analysis
426 and Kinetic Modeling. *Ind. Eng. Chem. Res.* **57**:10336–10344.

427 Huang J, Feng F, Wan M, Ying J, Li Y, Qu X, Pan R, Shen G, Li W. 2015. Improving
428 performance of flat-plate photobioreactors by installation of novel internal mixers optimized
429 with computational fluid dynamics. *Bioresour. Technol.* **182**:151–159.

430 Huang J, Li Y, Wan M, Yan Y, Feng F, Qu X, Wang J, Shen G, Li W, Fan J, Wang W. 2014.
431 Novel flat-plate photobioreactors for microalgae cultivation with special mixers to promote
432 mixing along the light gradient. *Bioresour. Technol.* **159**:8–16.

433 Kulkarni A V., Roy SS, Joshi JB. 2007. Pressure and flow distribution in pipe and ring spargers:
434 Experimental measurements and CFD simulation. *Chem. Eng. J.* **133**:173–186.

435 Lestinsky P, Vayrynen P, Vecer M, Wichterle K. 2012. Hydrodynamics of Airlift Reactor with
436 Internal Circulation Loop: Experiment vs. CFD Simulation. *Procedia Eng.* **42**:892–907.

437 Leupold M, Hindersin S, Gust G, Kerner M, Hanelt D. 2013. Influence of mixing and shear
438 stress on Chlorella vulgaris, Scenedesmus obliquus, and Chlamydomonas reinhardtii. *J.*
439 *Appl. Phycol.* **25**:485–495.

440 Luo HP, Al-Dahhan MH. 2004. Analyzing and Modeling of Photobioreactors by Combining
441 First Principles of Physiology and Hydrodynamics. *Biotechnol. Bioeng.* **85**:382–393.

442 Luo L, Liu F, Xu Y, Yuan J. 2011. Hydrodynamics and mass transfer characteristics in an
443 internal loop airlift reactor with different spargers. *Chem. Eng. J.* **175**:494–504.

444 Michels MHA, van der Goot AJ, Vermuë MH, Wijffels RH. 2016. Cultivation of shear stress
445 sensitive and tolerant microalgal species in a tubular photobioreactor equipped with a

centrifugal pump. *J. Appl. Phycol.* **28**:53–62.

Molina Grima E, Garcia Carnacho F, Sanchez Perez J a, Fernandez Sevilla JM, Acien Fernandez FG, Contreras Gomez a. 1994. in Light-Limited Chemostat Culture. *J. Chem. Technol. Biotechnol.* **61**:167–173.

de Mooij T, de Vries G, Latsos C, Wijffels RH, Janssen M. 2016. Impact of light color on photobioreactor productivity. *Algal Res.* **15**:32–42.

Mu Y, Yang H-Y, Wang Y-Z, He C-S, Zhao Q-B, Wang Y, Yu H-Q. 2015. The maximum specific hydrogen-producing activity of anaerobic mixed cultures: definition and determination. *Sci. Rep.* **4**:5239.

Pallas NR, Harrison Y. 1990. An automated drop shape apparatus and the surface tension of pure water. *Colloids and Surfaces* **43**:169–194.

Posten C. 2009. Design principles of photo-bioreactors for cultivation of microalgae. *Eng. Life Sci.* **9**:165–177.

Ranade V V., Tayalia Y. 2001. Modelling of fluid dynamics and mixing in shallow bubble column reactors: Influence of sparger design. *Chem. Eng. Sci.* **56**:1667–1675.

Ratchford IAJ, Fallowfield HJ. 1992. Performance of a flat plate, air-lift reactor for the growth of high biomass algal cultures. *J. Appl. Phycol.* **4**:1–9.

del Rio-Chanona EA, Ling X, Zhang D, Tang Y, Jing K, Yao C. 2017. Overproduction of L-tryptophan via simultaneous feed of glucose and anthranilic acid from recombinant Escherichia coli W3110: Kinetic modeling and process scale-up. *Biotechnol. Bioeng.* **115**:371–381.

del Rio-Chanona EA, Wagner JL, Ali H, Fiorelli F, Zhang D, Hellgardt K. 2019. Deep learning-based surrogate modeling and optimization for microalgal biofuel production and photobioreactor design. *AIChE J.* **65**:915–923.

Sforza E, Simionato D, Giacometti GM, Bertucco A, Morosinotto T. 2012. Adjusted light and dark cycles can optimize photosynthetic efficiency in algae growing in photobioreactors. *PLoS One* **7**:e38975.

Singh RN, Sharma S. 2012. Development of suitable photobioreactor for algae production – A review. *Renew. Sustain. Energy Rev.* **16**:2347–2353.

Sokolichin a., Eigenberger G, Lapin a. 2004. Simulation of Buoyancy Driven Bubbly Flow: Established Simplifications and Open Questions. *AIChE J.* **50**:24–45.

Su Z, Kang R, Shi S, Cong W, Cai Z. 2010. Study on the destabilization mixing in the flat plate photobioreactor by means of CFD. *Biomass and Bioenergy* **34**:1879–1884.

Sun Y, Huang Y, Liao Q, Fu Q, Zhu X. 2016. Enhancement of microalgae production by embedding hollow light guides to a flat-plate photobioreactor. *Bioresour. Technol.* **207**:31–38.

Thomas WH, Gibson CH. 1990. Effects of small-scale turbulence on microalgae. *J. Appl. Phycol.* **2**:71–77.

Wichmann J, Baier T, Wentnagel E, Lauersen KJ, Kruse O. 2018. Tailored carbon partitioning for phototrophic production of (E)-α-bisabolene from the green microalga Chlamydomonas reinhardtii. *Metab. Eng.* **45**:211–222.

Wilcox DC. 2006. Turbulence Modeling for CFD. Flintridge, CA, USA: DCW Industries. Turbulence Modeling for CFD.

Yang Z, Cheng J, Xu X, Zhou J, Cen K. 2016. Enhanced solution velocity between dark and light areas with horizontal tubes and triangular prism baffles to improve microalgal growth in a flat-panel photo-bioreactor. *Bioresour. Technol.* **211**:519–526.

Zhang D, Dechatiwongse P, del Rio-Chanona EA, Maitland GC, Hellgardt K, Vassiliadis VS. 2015a. Modelling of light and temperature influences on cyanobacterial growth and biohydrogen production. *Algal Res.* **9**:263–274.

Zhang D, Dechatiwongse P, Hellgardt K. 2015b. Modelling light transmission, cyanobacterial growth kinetics and fluid dynamics in a laboratory scale multiphase photo-bioreactor for biological hydrogen production. *Algal Res.* **8**:99–107.

Zhang D, Dechatiwongse P, del Rio-Chanona EA, Maitland GC, Hellgardt K, Vassiliadis VS. 2015c. Dynamic modelling of high biomass density cultivation and biohydrogen production in different scales of flat plate photobioreactors. *Biotechnol. Bioeng.* **112**:2429–2438.

Zhang K, Kurano N, Miyachi S. 2002. Optimized aeration by carbon dioxide gas for microalgal production and mass transfer characterization in a vertical flat-plate photobioreactor. *Bioprocess Biosyst. Eng.* **25**:97–101.

Nomenclature

A	cross-sectional area of PBR (m^2)
C_d	drag coefficient (1)
d_b	gas bubble diameter (m)
D_H	sparger hole diameter (mm)
D_s	sparger diameter (mm)
E_a	algae activation energy (kJ/mol)
E_b	algae deactivation energy (kJ/mol)
g	gravity vector (m/s^2)
h_l	unaerated liquid height (m)
I_0	incident light intensity ($\mu E/m^2/s$)
$I(z)$	local light intensity ($\mu E/m^2/s$)
k_i	photoinhibition term ($\mu E/m^2/s$)
k_s	photosaturation term ($\mu E/m^2/s$)
K_a	bubble scattering coefficient (1/m)
m_{gl}	mass transfer rate ($kg/m^3 \cdot s$)
N_H	number of sparger holes
p	pressure (Pa)
P	bisabolene production (µg/L)
P_h	pressure at the top of sparger holes (Pa)
P_H	sparger hole pitch (mm)
P_s	power input (W/m^3)
Q	gas volumetric flow rate (L/min)
Q_m	gas molar flow rate (mol/s)

R	gas constant (J/mol·K)
Re	Reynolds number (1)
T	temperature (K)
U	velocity vector (m/s)
U_g	gas velocity (m/s)
U_f	friction velocity (cm/s)
U_s	superficial gas velocity (m/s)
X	biomass concentration (g/L)
z	distance from light source (m)

Greek symbols

α	bisabolene synthesis rate (1)
ρ	density (kg/m^3)
φ	volume fraction (1)
μ	biomass specific growth rate (1/h)
μ_d	biomass specific decay rate (L/g/h)
μ_l	liquid viscosity (Pa·s)
μ_T	turbulent or eddy viscosity (Pa·s)
σ	surface tension coefficient (N/m)
τ	cell absorption coefficient (m^2/g)
τ_s	shear stress (Pa)

Subscripts

g	gas phase
l	liquid phase

552 **LIST OF TABLES**

555

Sparger design	Number of holes	Hole diameter (mm)	Recycling gas flow rate (L/min)
1	62	1	5
2	62	1	20
3	122	1	5
4	122	1	20
5	62	5	5
6	62	5	20
7	122	5	5
8	122	5	20

556 **Table 1.** Design configurations of sparger used in the study.

Sparger design	Productive volume (L)	Unproductive or dead zone volume (L)	Productivity loss (%)
1	101.29	18.69	15.59
2	45.55	74.43	62.04
3	118.00	1.99	1.66
4	72.41	47.58	39.65
5	107.42	12.57	10.48
6	46.03	73.96	61.64
7	115.83	4.16	3.475
8	79.30	40.69	33.91

557 **Table 2.** Effects of the different sparger designs on the PBR productivity.

LIST OF FIGURES

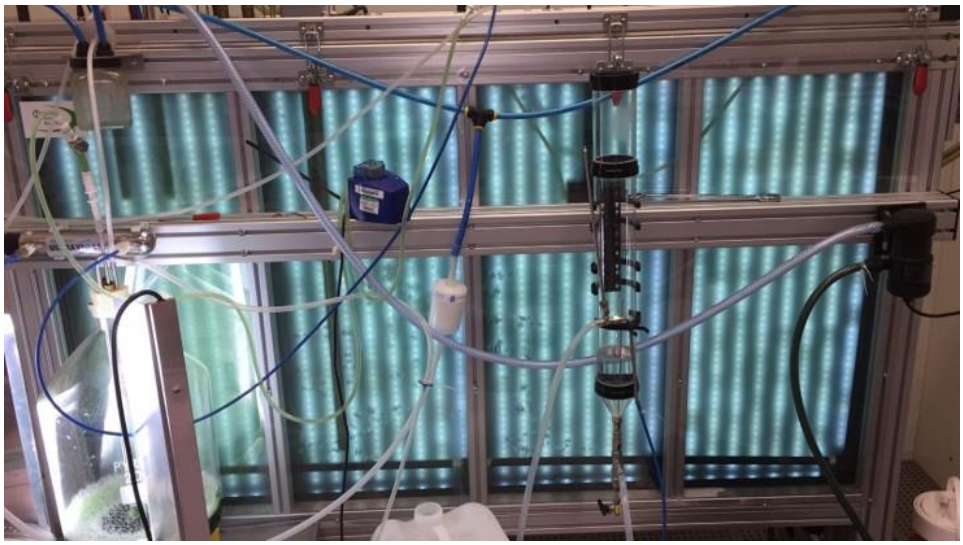

(**a**)

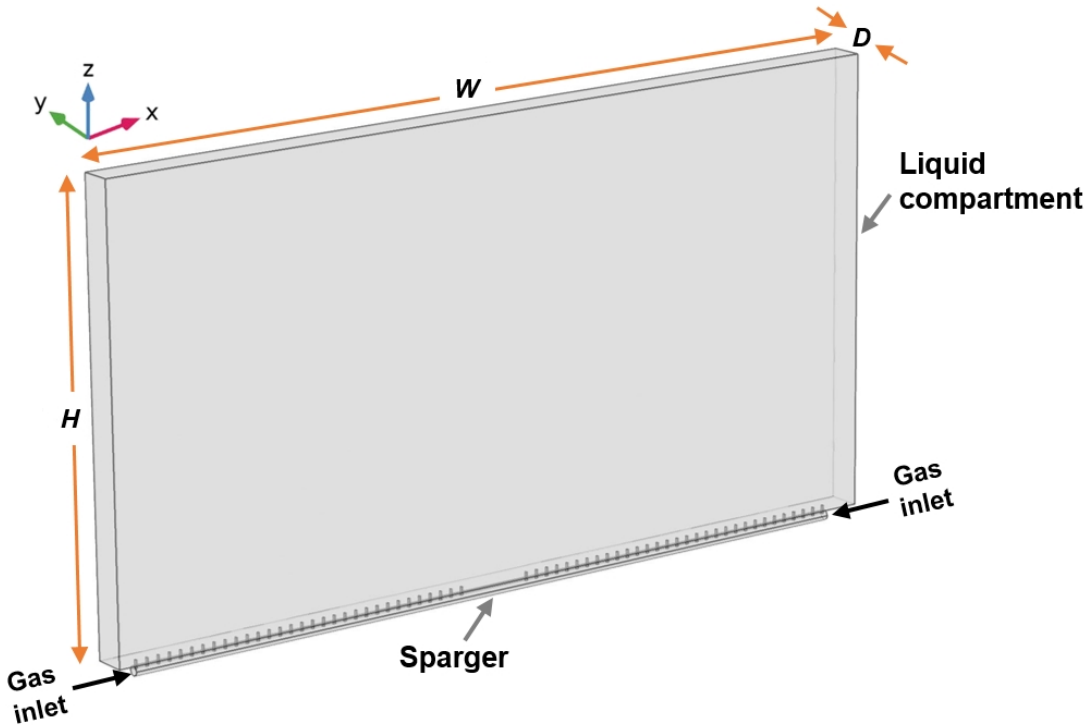

(**b**)

Figure 1. Experimental 120 L flat-plate closed photobioreactor (**a**) and its computational fluid dynamic (CFD) model (**b**) used in the simulations.

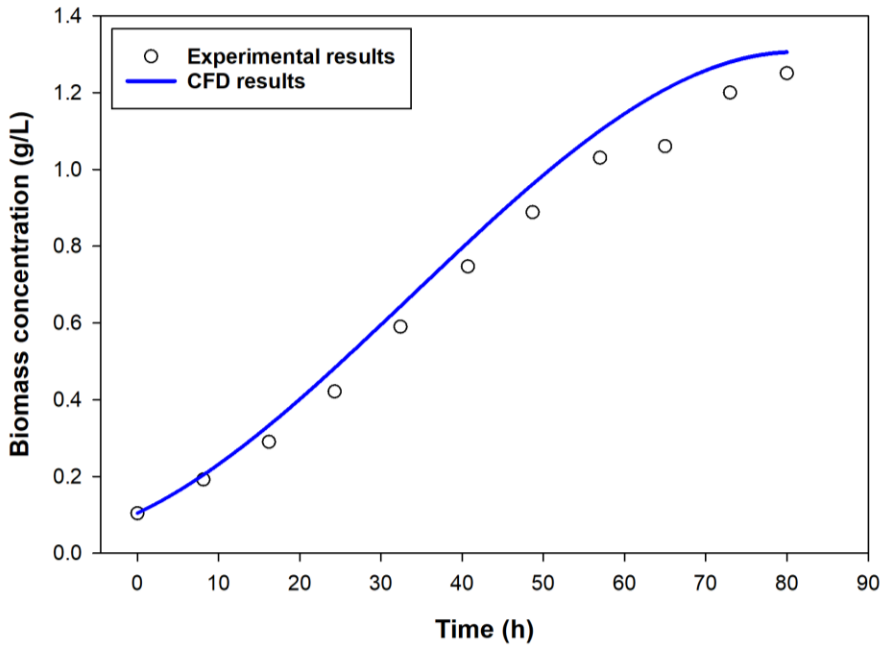

578

579 (**a**)

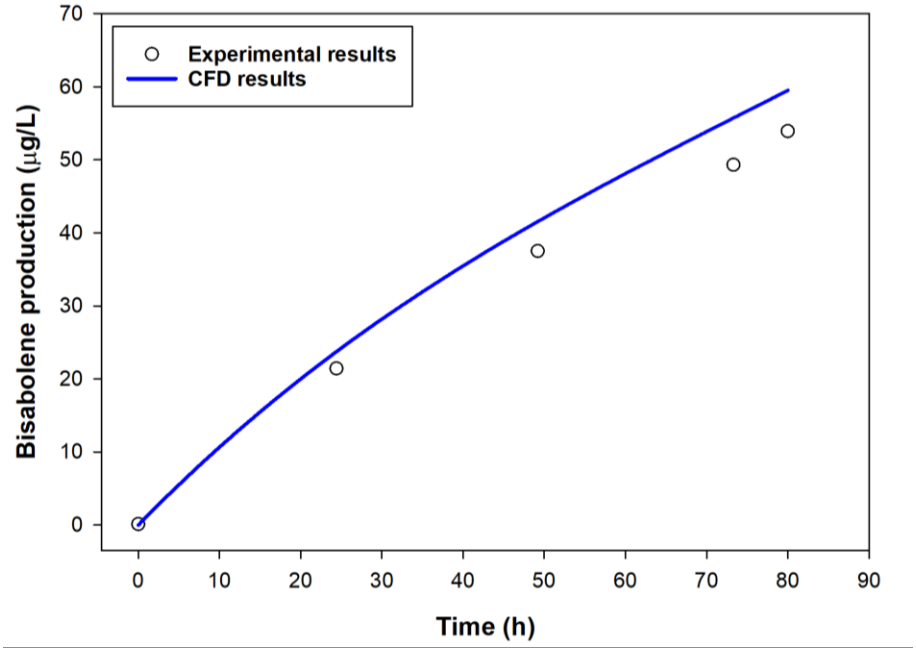

580

581 (**b**)

582 **Figure 2.** Comparison between the experimental and CFD results based on (**a**) biomass

583 concentration and (**b**) bisabolene production.

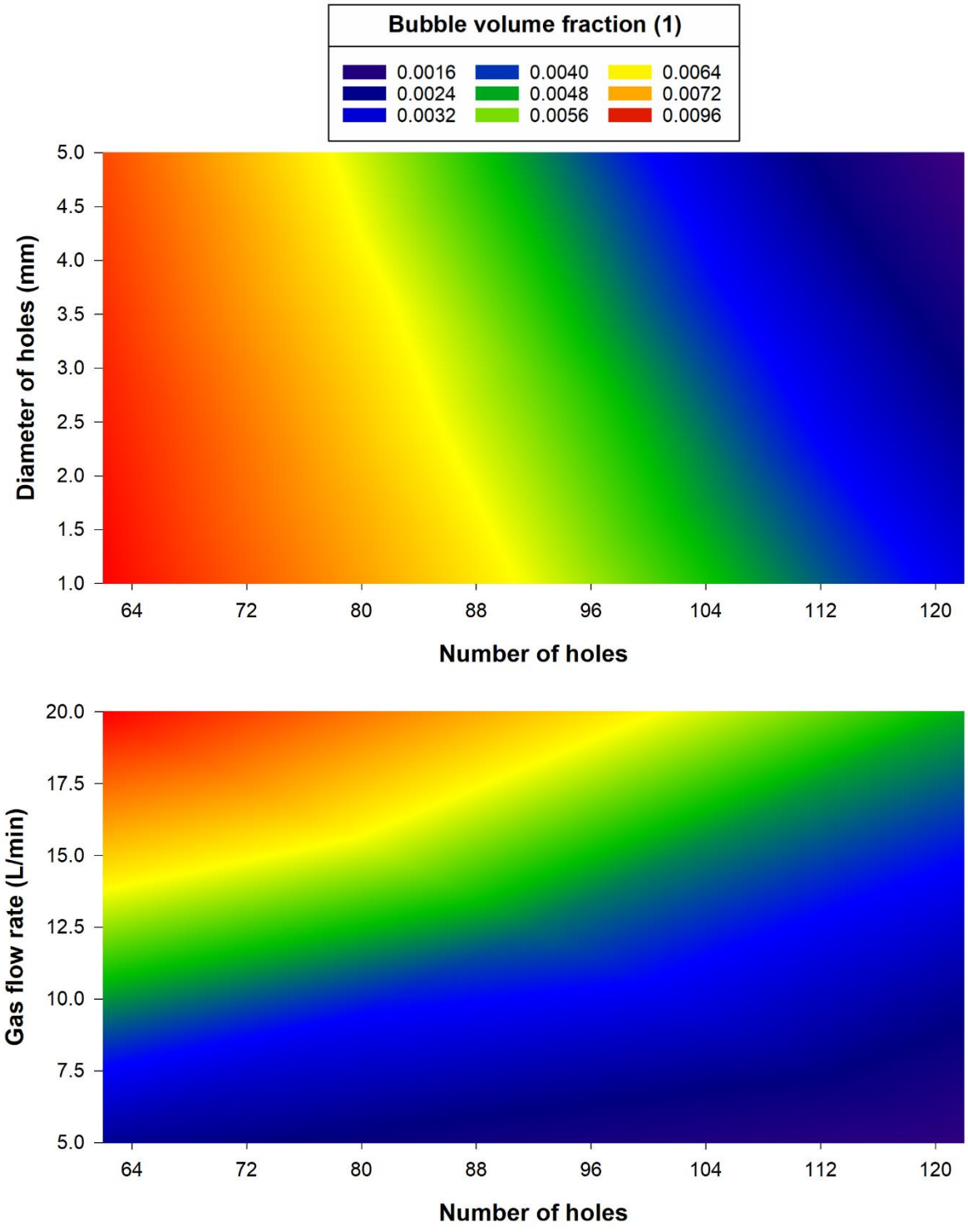

584

585 **Figure 3.** Gas bubble volume fraction with different numbers and diameters of sparger holes at

586 different gas recycling rates.

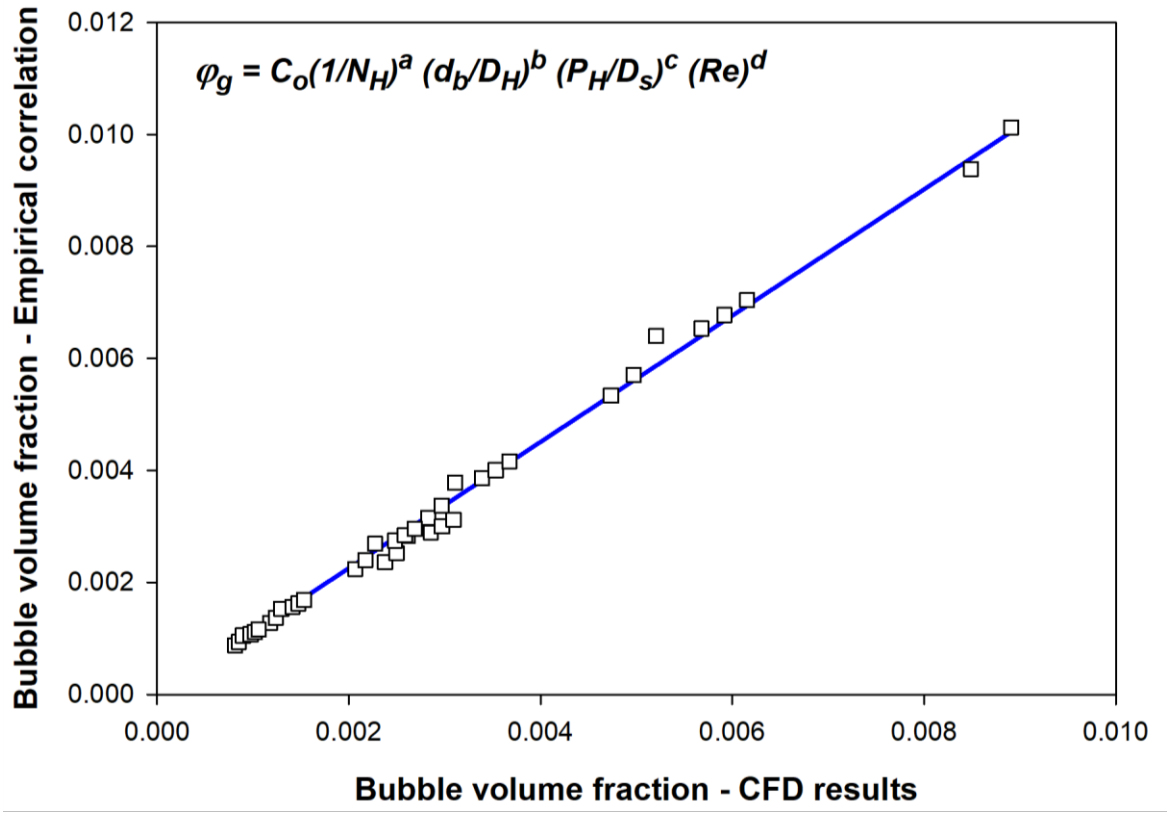

587

588 **Figure 4.** Comparison of the CFD data with the empirical correlation of bubble volume fraction

589 for different sparger designs.

590

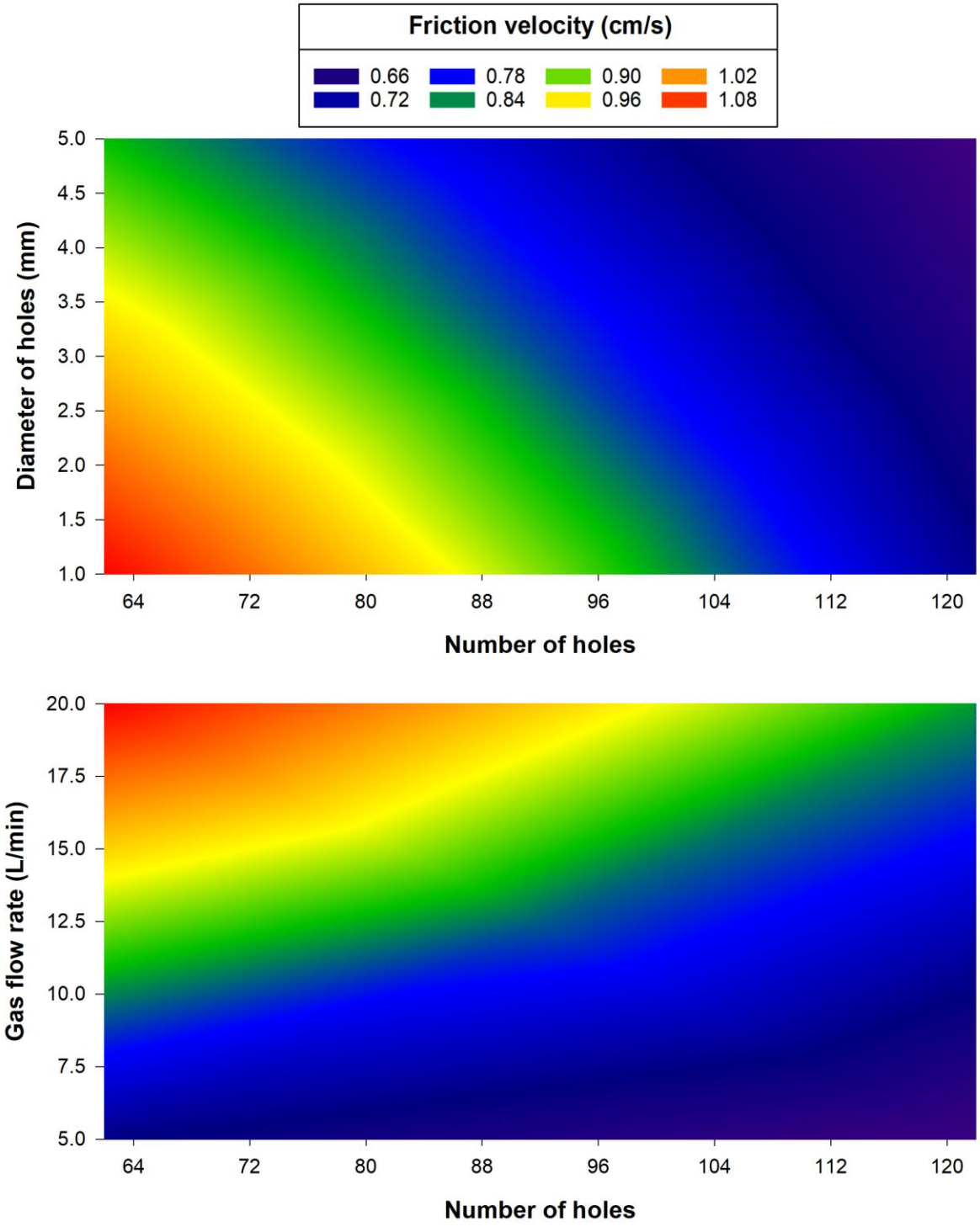

591

592 **Figure 5.** Friction velocity with different numbers and diameters of sparger holes at different gas

593 recycling rates.

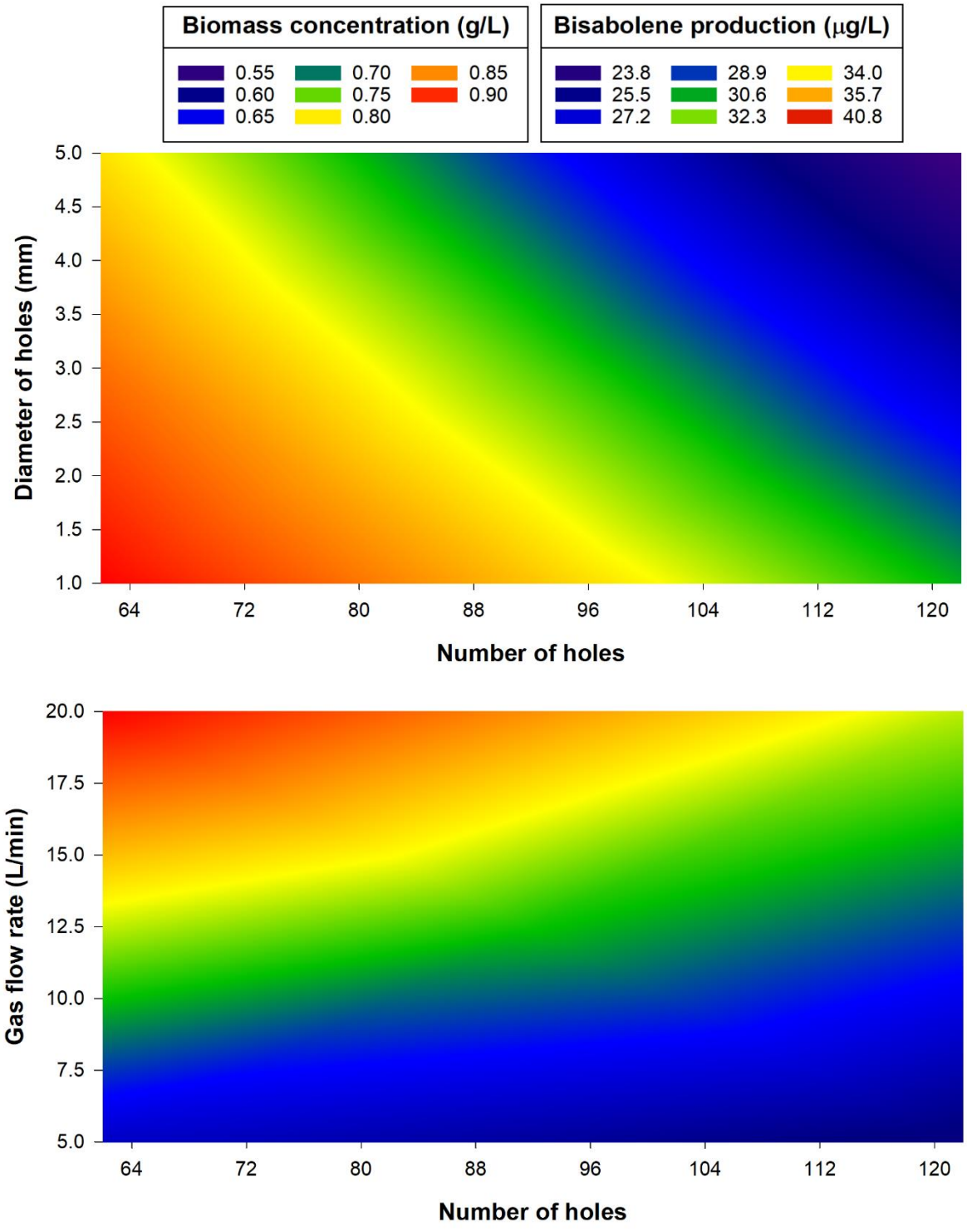

Figure 6. Biomass concentration and bisabolene production with different numbers and diameters of sparger holes at different gas recycling rates.